



# An improved generative adversarial network with modified loss function for crack detection in electromagnetic nondestructive testing

Lulu Tian<sup>2</sup> · Zidong Wang<sup>1</sup> · Weibo Liu<sup>1</sup> · Yuhua Cheng<sup>2</sup> · Fuad E. Alsaadi<sup>3</sup> · Xiaohui Liu<sup>1</sup>

Received: 30 May 2021 / Accepted: 14 July 2021 / Published online: 29 July 2021  
© The Author(s) 2021

## Abstract

In this paper, an improved generative adversarial network (GAN) is proposed for the crack detection problem in electromagnetic nondestructive testing (NDT). To enhance the contrast ratio of the generated image, two additional regulation terms are introduced in the loss function of the underlying GAN. By applying an appropriate threshold to the segmentation of the generated image, the real crack areas and the fake crack areas (which are affected by the noises) are accurately distinguished. Experiments are carried out to show the superiority of the improved GAN over the original one on crack detection tasks, where a real-world NDT dataset is exploited that consists of magnetic optical images obtained using the electromagnetic NDT technique.

**Keywords** Crack detection · Generative adversarial networks · Image segmentation · Image processing · Electromagnetic nondestructive testing

## Introduction

The past few decades have witnessed a great deal of research attention devoted to crack detection on industrial components such as the undercarriage of the plane and the bogie of the train. In general, most of the traditional crack detection methods are based on destructive testing which may cause secondary defects. The performance of the destructive testing methods is unsatisfactory especially when detecting the subsurface cracks that could grow in a persistent yet imperceptible way. To effectively detect both the surface and subsurface cracks, the nondestructive testing (NDT) techniques have been successfully applied to a variety of

industries such as aerospace, mechanical engineering, and transportation [44,51].

Recently, a large number of NDT methods have been developed using various testing methods (e.g. the ultrasonic testing, the laser shearography testing and the electromagnetic testing methods). Owing to their fast detection speed and high detection accuracy, electromagnetic testing methods have attracted particular research attention among the aforementioned testing methods. Typical electromagnetic testing methods include the pulsed eddy current array method [49], the pulsed eddy current thermography imaging method [11], and the magnetic optical imaging (MOI) method [7]. Up to now, electromagnetic testing methods have been widely studied and employed in a variety of practical systems [6,10]. For instance, the pulsed eddy current thermography imaging method has been employed in [6] to detect the surface crack for carbon fiber reinforced plastic material. In [10], the MOI method has been applied to detect both the surface and subsurface cracks in aircraft skins.

In electromagnetic NDT, the magnetic field of the crack area is different from that of the non-crack area. It should be mentioned that the magnetic field of the specimen mainly includes four parts, which are the magnetic field produced by the exciting circuit, the induced magnetic field (produced by the eddy current), the magnetic domain, and the magnetizing field (produced by the rust in the material and some

✉ Zidong Wang  
Zidong.Wang@brunel.ac.uk

Yuhua Cheng  
yhcheng@uestc.edu.cn

<sup>1</sup> Department of Computer Science, Brunel University London, Uxbridge, Middlesex UB8 3PH, UK

<sup>2</sup> School of Automation Engineering, University of Electronic Science and Technology of China, Chengdu 611731, Sichuan, China

<sup>3</sup> Department of Electrical and Computer Engineering, Faculty of Engineering, King Abdulaziz University, Jeddah 21589, Saudi Arabia

other factors). In this context, the obtained electromagnetic NDT images contain the real cracks and noises. To accurately detect the cracks in the electromagnetic NDT images, a seemingly natural idea is to apply image segmentation methods to segment the cracks [8,23,43].

As a powerful image processing technique, image segmentation has been widely utilized in many real-world applications, e.g. crack detection, fault diagnosis, medical imaging, and face recognition [45,48]. Among the popular image segmentation techniques, the threshold-based image segmentation technique has been widely used owing to its simplicity, fast processing speed and relatively small storage space. It is difficult to segment the cracks using traditional threshold-based image processing methods because of the influence of the noises in the electromagnetic images [5]. In recent years, a large number of machine learning algorithms have been developed and successfully exploited in a variety of research areas such as object detection, path planning, recommender system and image processing [1–3,8,9,16,22,23,29–31,40,43,53]. Due to their strong abilities in feature extraction, deep learning techniques (which are a powerful family of machine learning algorithms) have been successfully applied to NDT [4]. Although deep learning algorithms have achieved a great success in NDT, the performance of the deep learning algorithms is highly related to the quantity and quality of the training data. To be specific, a large amount of data is required for training an effective deep learning model.

In deep learning, generative adversarial networks (GANs) have received enormous attention from various computer science communities (e.g. computer vision, signal processing, and image processing) because of their strong abilities in data generation [32,39,41]. In recent years, GANs have shown competitive performance in crack detection and fault diagnosis, see in [12,13,38]. In [13], a deep convolutional GAN has been utilized to automatically detect the cracks in fabrics. An improved least-square GAN has been put forward in [38] for rail crack detection. In [12], the GAN-based method has been developed for detecting the subsurface cracks in the steel material. Notice that most current GAN-based crack detection methods have been applied to detect the cracks on natural optical images.

In the context of electromagnetic crack detection, there appear to be two challenging issues: (1) the obtained electromagnetic image is not natural optical image, and the contrast ratio of the electromagnetic image is low, which makes it difficult to accurately distinguish the real cracks and noises; and (2) the actual position of the crack is hard to be identified. In this paper, it would make practical sense to develop an advanced GAN for crack detection of the electromagnetic images so as to: (1) reduce the influence of the noises in electromagnetic images; and (2) enhance the contrast ratio of the electromagnetic images for image segmentation.

Motivated by the above discussions, in this paper, we endeavor to propose an improved GAN-based crack detection method to handle the electromagnetic NDT crack detection problem. *The main contributions of this paper are highlighted as follows: (1) a GAN-based method is put forward for crack detection of the magnetic optical images for the first time; (2) a novel loss function of the GAN is designed to reconstruct the magnetic optical images, where the designed penalty terms are introduced in the loss function to enhance the contrast ratio of the images; and (3) the proposed GAN-based crack detection method is successfully applied to a real-world NDT dataset with promising results.*

The rest of this paper is organized as follows. The background of electromagnetic NDT is introduced in “Background of electromagnetic NDT”. In “The improved generative adversarial network”, the proposed GAN-based image reconstruction method is discussed. Experiment results and discussions are presented in “Experiment results”. Finally, conclusions are drawn in “Conclusion”.

## Background of electromagnetic NDT

### Mechanism of electromagnetic NDT

In electromagnetic NDT, the crack information of the conductive specimen is highly related to the magnetic field induced by the eddy current. The process of the electromagnetic testing approach is shown in Fig. 1. It is known that the path of the eddy current will be changed due to the existing of cracks in the specimen, which leads to the change of the distribution and magnitude of the induced magnetic field “ $B_2$ ” as shown in Fig. 1.

It should be pointed out that the magnitude of the magnetic field at the edge of the crack area is bigger than that at other areas. In the electromagnetic NDT images, the area with bigger pixel values can be recognized as the crack area with

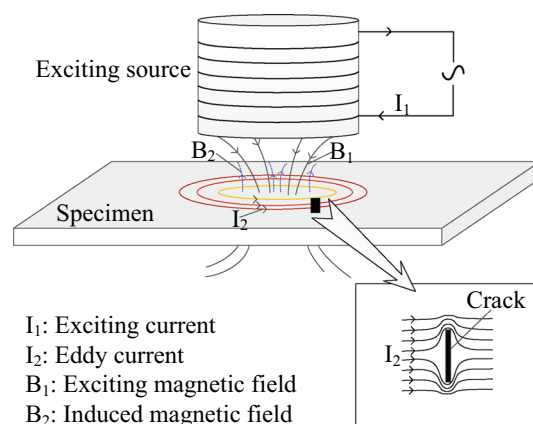


Fig. 1 The schematic diagram of the electromagnetic testing method

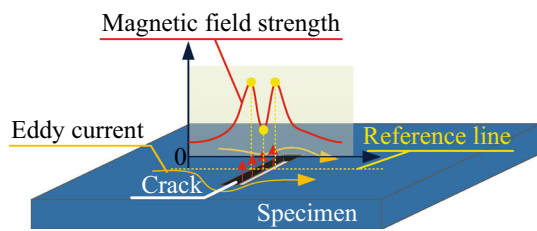


Fig. 2 Magnetic field around the crack area

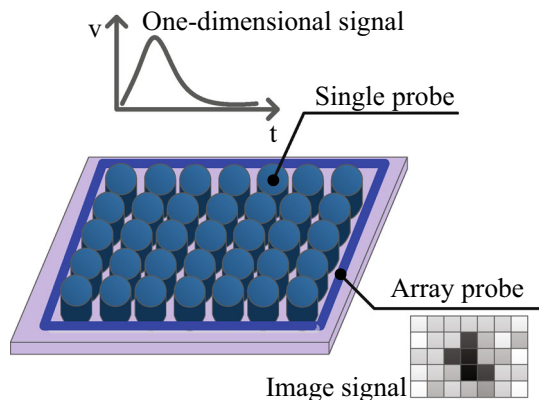


Fig. 3 The eddy current thermography method for detecting the magnetic field

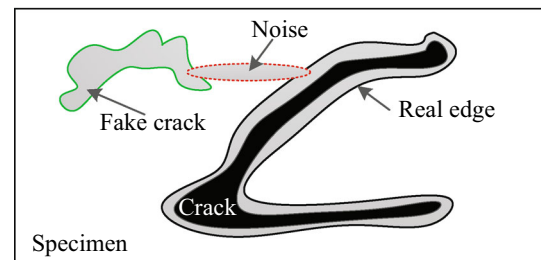
high probability. The diagram of the magnetic field around the crack area is shown in Fig. 2.

In recent years, many electromagnetic-based imaging NDT methods (e.g. the magnetic optical imaging (MOI) method and the eddy current pulsed thermography method) have been proposed due to the rapid development of sensors for detecting the electromagnetic signal. As a popular electromagnetic NDT technique, the eddy current thermography method uses multiple probes to detect the magnetic field, which is shown in Fig. 3.

### Characteristics of the electromagnetic images

The characteristics of electromagnetic NDT images are summarized as follows:

- (1) The amount of data is small. In the experimental situation, the NDT methods are employed to detect the cracks in the specimens. Although the detection accuracy of the NDT method is satisfactory, the computational cost of the NDT method is high and the cost of the NDT method is expensive. As a result, the number of the obtained electromagnetic images is limited.
- (2) The shape of the cracks is unpredictable. Generally, the magnetic field of the specimen is affected by various factors (including the magnetic field produced by the exciting circuit and the induced magnetic field). In this



- The determinate region of crack
- The similar grayscales

Fig. 4 The influence of the noise in crack detection

context, the detected magnetic field of the specimen is different between two separate NDT tests, which leads to the variation of the crack shape.

- (3) The existence of noise in electromagnetic images affect the performance of crack detection. In electromagnetic NDT, noises would lead to the so-called “fake crack” areas. It is difficult to distinguish the real crack area and the “fake crack” area because the pixel values of the magnetic field of the real crack and “fake crack” areas are very similar. The influence of the noise in crack detection is shown in Fig. 4.

According to the characteristics of electromagnetic images, it is challenging to employ traditional image segmentation methods to accurately distinguish the crack area and the “fake crack” area. Therefore, it is of practical importance to deploy an advanced image segmentation method. Owing to their strong abilities in feature extraction and data generation, GANs have shown competitive performance in crack detection. Motivated by the above discussions, a novel GAN-based method is developed in this paper to reconstruct the electromagnetic image for image segmentation so as to detect the cracks.

### The improved generative adversarial network

In this section, the framework of the improved GAN and the developed GAN-based crack detection approach are presented. The designed loss function of the improved GAN is also introduced.

### The proposed GAN-based approach

The original GAN consists of two competing networks: a generator and a discriminator. The generator aims to generate fake samples as *real* as possible. The purpose of the discriminator is to distinguish the real samples and the gen-

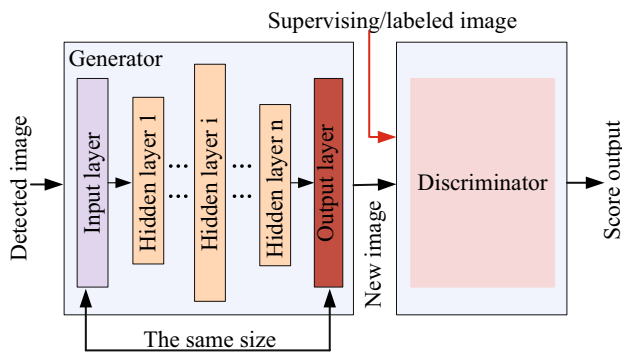


Fig. 5 The structure of the GAN

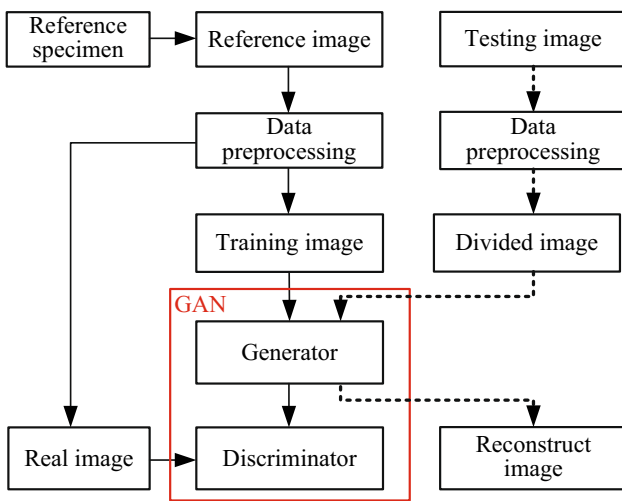


Fig. 6 The framework of the developed GAN-based crack detection method

erated fake samples. The framework of the original GAN is shown in Fig. 5.

In the original GAN, the input of the generator is random noise, and the input of the discriminator includes two parts (which are the output of the generator and the real data). In this paper, the training data of the GAN includes the electromagnetic images (which is also called as the reference images) and the preprocessed images.

The framework of the proposed GAN-based crack detection approach is depicted in Fig. 6. In this paper, each electromagnetic image is divided into a number of images with a smaller size than that of the raw image, which contributes to the improvement of the learning process of the GAN. The output images of the generator are then combined together to reconstruct the electromagnetic image.

### The modified loss function of the GAN

In the proposed GAN-based crack detection method, we aim to apply the improved GAN to (1) distinguish the crack area and “fake crack” area; and (2) reduce the influence of noises.

To achieve the aforementioned two objectives, a new loss function is put forward where two designed penalty terms are added in the loss function to enhance the contrast ratio of the generated image.

The relationship between the training image and the generated output image is shown as follows:

$$X = G(I) \tag{1}$$

where  $G(\cdot)$  stands for the generator,  $I$  denotes the training image, and  $X$  represents the output image of the generator.

The training process of a GAN can be treated as a minimax two-player game. The loss function of the original GAN for image processing is shown as follows:

$$L_a = \mathbb{E}_{S \sim \mathbb{P}_r} [\log D(S)] + \mathbb{E}_{I \sim \mathbb{P}_c} [\log(1 - D(G(I)))] \tag{2}$$

where  $\mathbb{P}_c$  is the pixel value distribution of the training image;  $\mathbb{P}_r$  is the pixel value distribution of the real image;  $S$  is the input of the discriminator;  $G(\cdot)$  represents the generator and  $D(\cdot)$  is the discriminator. The pixel value of the output image obtained by the generator is in the range of (0, 1).

To enhance the contrast ratio of the reconstructed electromagnetic images, two designed penalty terms are introduced in the loss function of the GAN. By employing the penalty terms, the noise in the raw electromagnetic images is removed, which contributes to the crack detection. The loss function of the improved GAN is shown as follows:

$$L_i = L_a + \mathbb{E}_{I \sim \mathbb{P}_c} \left[ \lambda_1 \|\mathbf{1} - I\|_F \|G(I)\|_F + \lambda_2 \frac{\|I\|_F}{\|G(I)\|_F} \right] \tag{3}$$

where  $\lambda_1$  and  $\lambda_2$  are penalty factors;  $\|\cdot\|_F$  is the Frobenius norm defined by  $\|A\|_F = \sqrt{\sum_{i,j} A_{i,j}^2}$ ;  $\mathbb{E}_{I \sim \mathbb{P}_c} [\|\mathbf{1} - I\|_F \|G(I)\|_F]$  is utilized to shrink the points with small pixel values; and

$$\mathbb{E}_{I \sim \mathbb{P}_c} \left[ \frac{\|I\|_F}{\|G(I)\|_F} \right]$$

is designed to enlarge the points with large pixel values.

The purpose of the improved GAN is to solve the following minimax problem

$$\min_G \max_D L_i$$

where the training process of such improved GAN is described in Fig. 7. It should be pointed out that the generator is trained once at each iteration in this work.

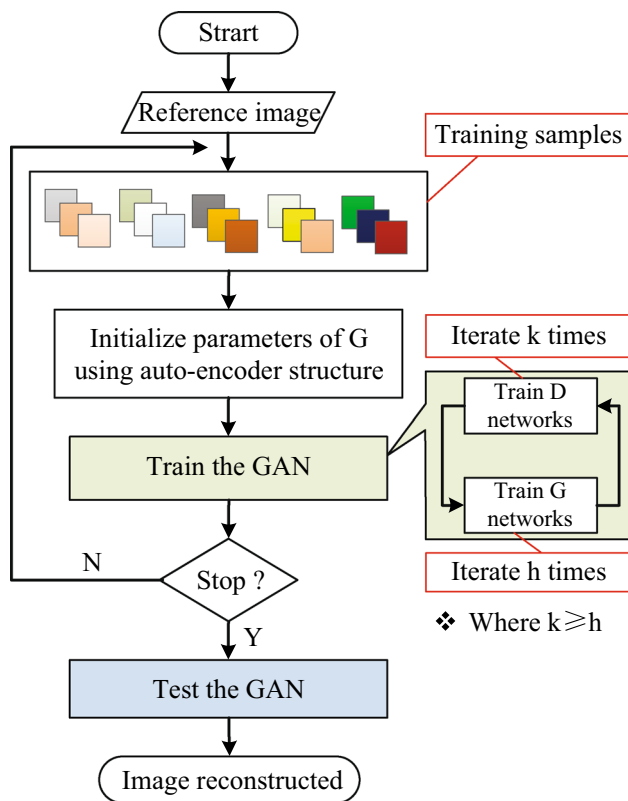


Fig. 7 The flowchart of the algorithm G: generator of GAN; D: discriminator of GAN

### Experiment results

In this paper, the proposed GAN-based method is pre-trained to deal with the magnetic optical images which are captured through the MOI test. In this section, the hardware of the MOI test is discussed, and data preprocessing is presented. In addition, experiment results are presented to demonstrate the superiority of the proposed GAN-based crack detection method.

### Experiment setup

Served as a popular NDT technique, the MOI detection mechanism includes an optical system and an excitation system. The hardware of the MOI detection mechanism is depicted in Fig. 8.

In the MOI test, the crack information is influenced by the magnetic field. The optical system is utilized to detect the magnetic field that is distributed on the surface of the specimen. The polarizing films, i.e., the polarizer and the analyzer, are the most important components of the optical system. The polarizer is used to produce the polarized laser light, and the analyzer is utilized to filter the polarized light (which is rotated after interacting with the magnetic field). The charge-coupled device camera is adopted to record the

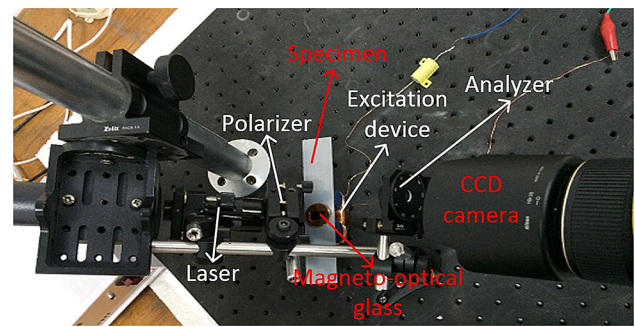


Fig. 8 Hardware of the MOI detection mechanism

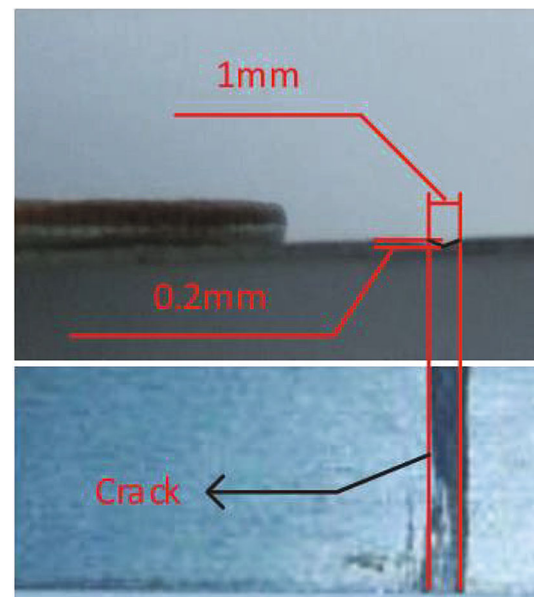


Fig. 9 The specimens used in the experiment

polarized light which contains the magnetic field information (especially the magnetic field induced by the crack). In our experiment, the specimens include two ferromagnetic thin plates. The ferromagnetic thin plate with the “Z” shape crack is utilized for the training process, and the other specimen with a scratch crack (1 mm width and 0.2 mm depth) is used for the testing process. The specimens are shown in Fig. 9.

### Data preprocessing

As a challenge in deep learning, a large amount of data is required for training satisfactory deep neural networks. Unfortunately, it is difficult to produce a large number of electromagnetic images for crack detection due to the high cost of the electromagnetic NDT technique. In this paper, data preprocessing is employed to produce effective training data.

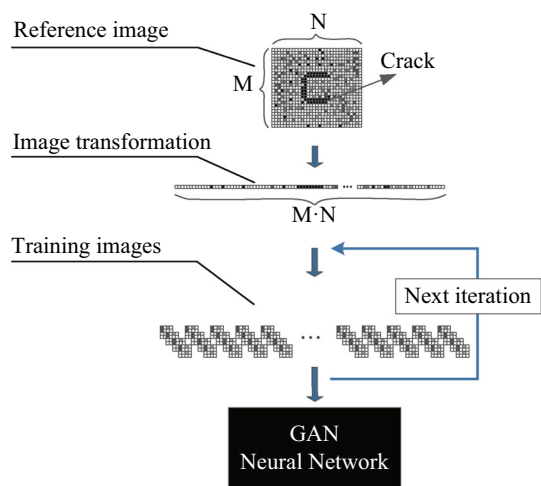


Fig. 10 The process of producing training images for GANs

The procedure of data preprocessing is given as below:

- (1) Initialization: Select the reference images which contains crack, fake crack and background areas. Then, normalize the selected images (with the size of  $M$  rows and  $N$  columns).
- (2) Vectorization: Convert each normalized image into a separate one column vector.
- (3) Training image selection: Randomly select  $m \cdot n$  ( $m < M, n < N$ ) elements from an arbitrary vector obtained in (2). Then, convert the  $m \cdot n$  elements to a  $m$  by  $n$  matrix as a training image.
- (4) Repeat (3) till a number of training images are obtained.

The process of the training image selection is shown in Fig. 10.

The purpose of the training image selection is to choose effective electromagnetic images that include the crack area, the non-crack area and the “fake crack” area. Moreover, the size of the training images is reduced by comparing with that of the electromagnetic images, which improves the efficiency of the training process. Notice that the selected electromagnetic images need to be binarized so as to obtain the ground truth information. The preprocessed images are also called as the *real images* in this paper for training the GANs. Particularly, the electromagnetic images are also preprocessed according to experiment experience and details can be seen in [7].

To sum up, a pair of training images of the GAN consist of one reference image and the corresponding real image. Then, the training images are cropped into images with a smaller size comparing with that of the raw images. As shown in Fig. 11, an MOI image (which is also known as a reference image) is obtained using the electromagnetic NDT technique.

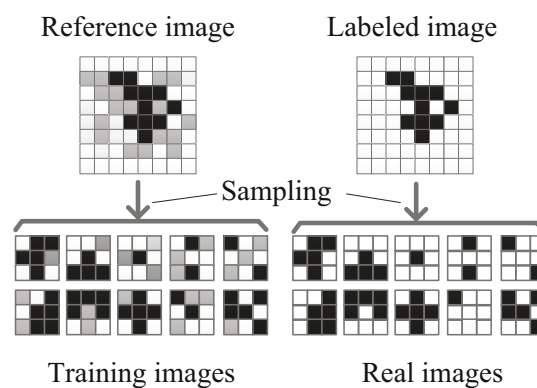


Fig. 11 The method of sampling training data

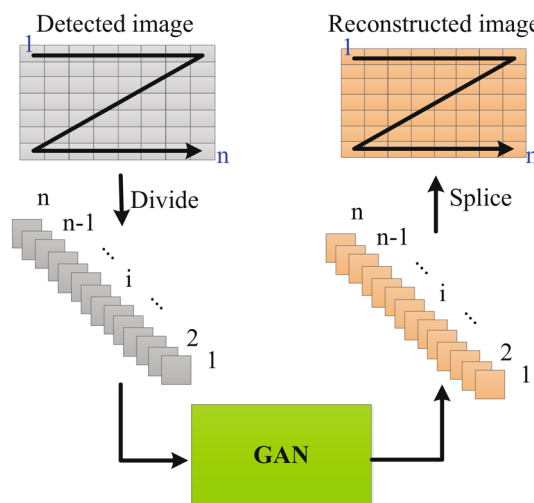
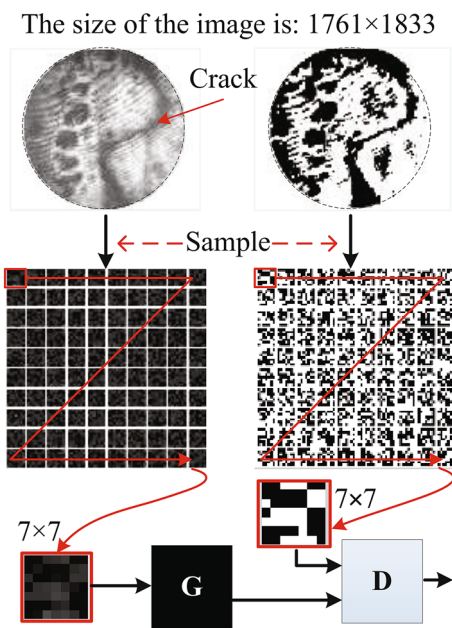


Fig. 12 The testing process

The MOI image is then binarized to obtain the real image, where the pixel value of the crack area is 1 and the pixel value of other area is 0.

In the testing process, the testing images are preprocessed into the same size as the training images. To be specific, the testing images are divided into sub-images to feed the generator. The output images of the generator are then spliced together so as to obtain the reconstructed images. The strategy of the testing process is depicted in Fig. 12.

The pre-training technique is widely used in deep learning to enhance the generalization ability of the deep neural networks [15]. To improve the feature learning and generalization abilities of the GAN, an auto-encoder (AE) is employed to pre-train the generator. In addition, the pre-training process contributes to a faster convergence for the GAN training process than the standard training process.



**Fig. 13** The training data of the discriminator G; generator of GAN; D: discriminator of GAN

## Results and analysis

The magnetic optical images are preprocessed by extracting the circle area that is only covered by the laser. The training data of the discriminator is displayed in Fig. 13.

The size of the raw magnetic optical image is  $1761 \times 1833$ . In this paper, 60,000 training images are generated with the size of  $7 \times 7$  based on the aforementioned preprocessing method. The labels of the pixels in the training images are obtained according to [7]. Each training image and its corresponding real image form a pair of training data. In the improved GAN, the “ReLU” function is chosen as the activation function of the hidden layers, and the “Sigmoid” function is utilized as the activation function of the output layers. The batch size is set to be 100. The hyperparameters  $\lambda_1$  and  $\lambda_2$  are set up to be 0.8 and 0.2 according to experiment experience.

The testing data is the magnetic optical image of the specimen with the scratch crack. The testing image is displayed in Fig. 14. In Fig. 14, the sub-figures (a), (b), and (c) represent the magnetic optical image, the normalized image, and the image processed using the “Sigmoid” function with (b) as the input, respectively. The sub-figures (d), (e), and (f) denote the pixel value distributions of (a), (b), and (c), respectively. It should be pointed out that the crack area also include noise, which is called as the “fuzzy area” as shown in (d). In the “fuzzy area”, there are a large number of points with high pixel values even when the image is processed using different image processing methods and their results are shown in (e) and (f). As such, it is difficult to choose a suitable threshold to segment the magnetic optical images for

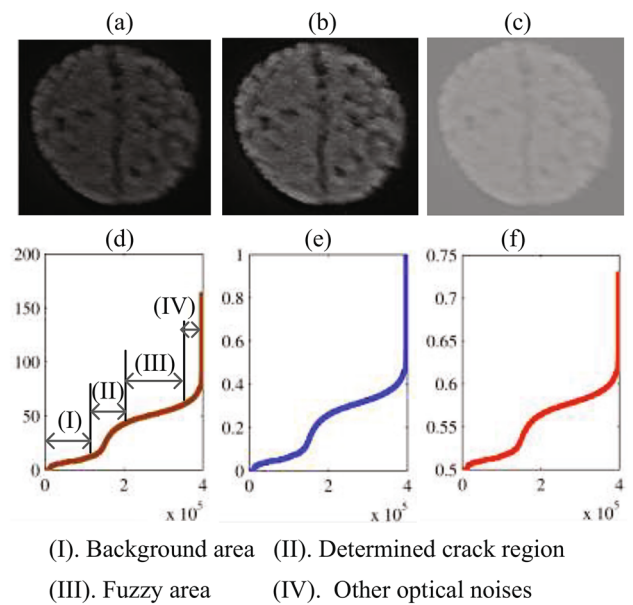


**Fig. 14** **a** Magnetic optical image; **b** normalized **a**; **c** processed **b** with the “Sigmoid” function; **d** pixel distribution of **a**; **e** pixel distribution of **b**; **f** pixel distribution of **c**

crack detection. Furthermore, the tail of pixel distribution in images (d), (e), and (f) is high and sharp, which leads to a big value as the threshold. Therefore, the performance of crack detection using such a big value as a threshold is poor.

To eliminate the noise and identify the crack area accurately, the improved GAN-based method is developed to reconstruct the magnetic optical images. The designed loss function enhances the contrast ratio of the magnetic optical images in the training process. In Fig. 15, the reconstructed images are displayed. In Fig. 15a, b are output images of the generator trained using the loss function (2), and image (c) represents the output image of the generator trained using the designed loss function (3). In Fig. 15d–f are the binary images (using the threshold of 0.6) of (a), (b), and (c), respectively.

It can be seen in Fig. 15 that (a) and (b) are generated using two GANs (with different hidden layer numbers) trained by using the same loss function (2). Figure 15c is generated using the proposed GAN with the designed loss function. It can be seen that noise exists in both the reconstructed images and the binary images, which affects the crack detection. In (c), the noise is largely reduced using the proposed improved GAN. The contrast ratio of the reconstructed image (c) is high, which indicates that the proposed GAN-based method performs better than the traditional GAN-based methods.

In Fig. 16, the pixel distribution of reconstructed images (a), (b), and (c) in Fig. 15 are displayed. Comparing the curves of “result 1” and “result 2” in Fig. 16 with that of (d), (e), and (f) in Fig. 14, the pixel distribution becomes smooth, especially in the tail of the curves. In addition, the changing rates of the curves of “result 1” and “result 2” are big in the

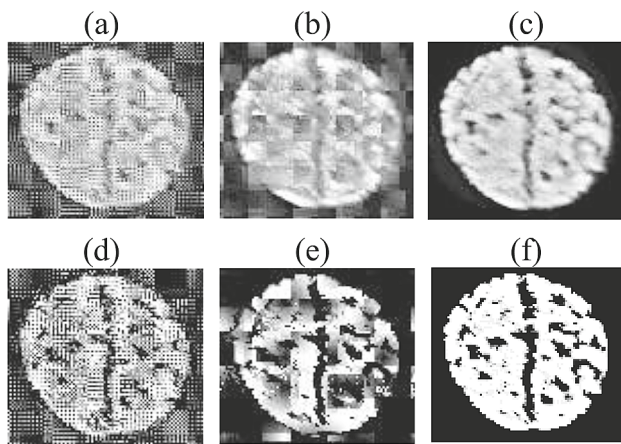


**Fig. 15** **a** Result 1 using loss function (2); **b** result 2 using loss function (2); **c** result using loss function (3); **d** the binarization of image **a** using the threshold 0.6; **e** the binarization of image **b** using the threshold 0.6; **f** the binarization of image **c** using the threshold 0.6

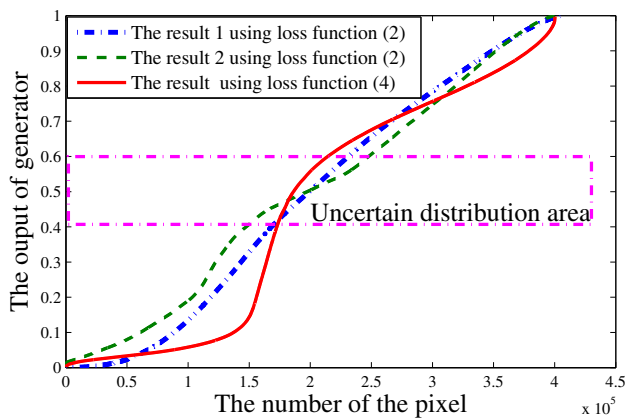


**Fig. 16** The pixel distributions of reconstructed image

middle area, and small in the end area, which indicates that the pixels are easy to be classified.

As shown in the curves “result 1” and “result 2”, the number of pixels in the uncertain area is still huge so that the dynamic range of the threshold-selection is big which may lead to the low crack identification accuracy. Using the loss function (3) to train the GAN, the distribution of the pixel value is sharp in the uncertain area and smooth in the end. In this case, there are very few pixels in the uncertain area which makes it easier to find an appropriate threshold, as shown in Fig. 16. To summarize, the GAN trained using the proposed loss function contributes to a better image segmentation than that of the original loss function.

To comprehensively evaluate the performance of the improved GAN-based crack detection method, a single pixel point is utilized as a training image. The corresponding experiment results are shown in Fig. 17.

It can be seen in Fig. 17 that the reconstructed image (a) and its binary image (b) show that the noise is reduced and

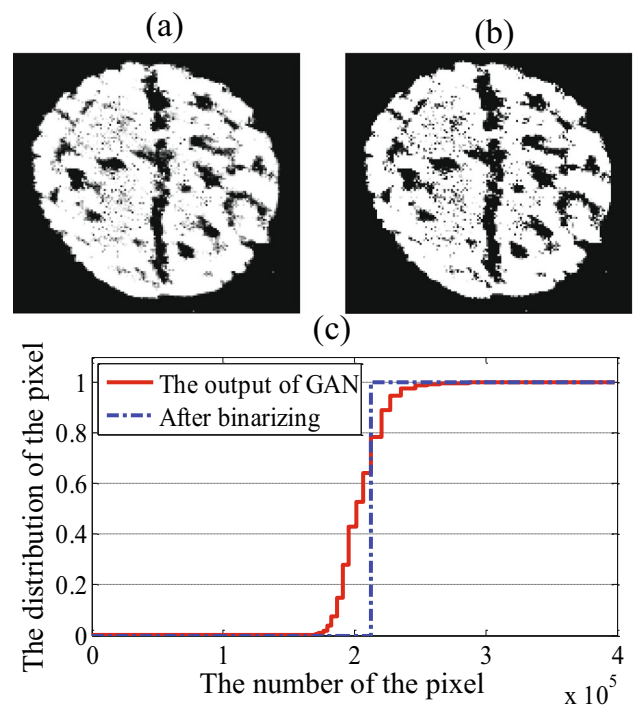


**Fig. 17** The result using  $1 \times 1$  sampled image

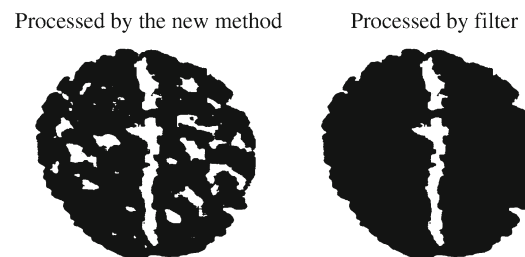


**Fig. 18** Crack extraction using the reconstructed image

the performance of the image segmentation is satisfactory. Figure 17c presents that the pixels are classified appropriately because most of the pixel value of the points approach to 0 (as shown by the black area) or 1 (as shown by the white area of the image). The distribution curve of image (a) is almost vertical in the uncertain area by comparing with that of binary image (b), which indicates that the performance of the reconstructing process is satisfactory.

According to previous research on the magnetic optical images [36,37], it is simple to extract the crack area depending on the reconstructed image as shown in Fig. 18. In particular, the shape/contour of the crack is identified, and the location of the crack in the specimen is detected, which contributes to the fault diagnosis and maintenance of equipment.



## Conclusion

In electromagnetic NDT, crack detection depends on the features of the imaging mechanism instead of the geometric features (such as the shape and length of the crack). In this paper, an improved GAN-based crack detection method has been proposed for electromagnetic NDT by analyzing the magnetic optical images. Data preprocessing has been employed to improve the generalization ability of the improved GAN, which overcomes the problem of lacking training images. Two designed penalty terms have been introduced in the loss function to enhance the contrast ratio of the reconstructed images and reduce the noises in the MOI images. Experiment results have shown that the improved GAN outperforms the standard GAN for reconstructing the magnetic optical images, and the developed GAN-based crack detection method has demonstrated satisfactory performance in detecting the cracks in magnetic optical images. In the future, we aim to (1) employ our proposed GAN-based crack detection for other NDT methods such as thermal imagery detection, ultrasound detection and X-ray imaging detection; (2) deploy evolutionary computation methods to optimize the parameter selection in the GAN-based crack detection system [24–27]; (3) employ signal processing and state estimation methods to investigate the stability of the NDT process [17, 19–21, 28, 34, 35, 42, 46, 54]; and (4) design an advanced control strategy to improve the detection accuracy and detection rate of the GAN-based crack detection system [14, 18, 33, 47, 50, 52, 55, 56].

**Acknowledgements** This research work was funded by Institutional Fund Projects under Grant no. (IFPIP-218-135-1442). Therefore, the authors gratefully acknowledge technical and financial support from the Ministry of Education and King Abdulaziz University, Jeddah, Saudi Arabia. This work was also supported in part by the National Natural Science Foundation of China under Grants 61873148, 61933007 and 61903065, the China Postdoctoral Science Foundation under Grant 2018M643441, the Royal Society of the UK, and the Alexander von Humboldt Foundation of Germany.

## Declarations

**Conflict of interest** On behalf of all authors, the corresponding author states that there is no conflict of interest.

**Open Access** This article is licensed under a Creative Commons Attribution 4.0 International License, which permits use, sharing, adaptation, distribution and reproduction in any medium or format, as long as you give appropriate credit to the original author(s) and the source, provide a link to the Creative Commons licence, and indicate if changes were made. The images or other third party material in this article are included in the article's Creative Commons licence, unless indicated otherwise in a credit line to the material. If material is not included in the article's Creative Commons licence and your intended use is not permitted by statutory regulation or exceeds the permitted use, you will need to obtain permission directly from the copyright holder. To view a copy of this licence, visit <http://creativecommons.org/licenses/by/4.0/>.

## References

- Bu Z, Li H-J, Zhang C, Cao J, Li A, Shi Y (2019) Graph K-means based on leader identification, dynamic game and opinion dynamics. *IEEE Trans Knowl Data Eng* 32(7):1348–1361
- Cao J, Bu Z, Gao G, Tao H (2016) Weighted modularity optimization for crisp and fuzzy community detection in large-scale networks. *Phys A Stat Mech Appl* 462:386–395
- Cao J, Wu Z, Mao B, Zhang Y (2013) Shilling attack detection utilizing semi-supervised learning method for collaborative recommender system. *World Wide Web J Internet Web Inf Syst* 16(5–6):729–748
- Chen FC, Jahanshahi MR (2017) NB-CNN: deep learning-based crack detection using convolutional neural network and Naïve Bayes data fusion. *IEEE Trans Ind Electron* 65(5):4392–4400
- Cheng HD, Wang J, Hu YG, Glazier C, Shi XJ, Chen XW (2001) Novel approach to pavement cracking detection based on neural network. *Transp Res Rec* 1764(1):119–127
- Cheng L, Tian GY (2011) Surface crack detection for carbon fiber reinforced plastic (CFRP) materials using pulsed eddy current thermography. *IEEE Sens J* 11(12):3261–3268
- Cheng Y, Tian L, Yin C, Huang X, Bai L (2016) A magnetic domain spots filtering method with self-adapting threshold value selecting for crack detection based on the MOI. *Nonlinear Dyn* 86(2):741–750
- Cheng Y, Tian L, Yin C, Huang X, Cao J, Bai L (2018) Research on crack detection applications of improved PCNN algorithm in moi nondestructive test method. *Neurocomputing* 277:249–259
- Cui Y, Liu Y, Zhang W, Alsaadi FE (2021) Sampled-based consensus for nonlinear multiagent systems with deception attacks: the decoupled method. *IEEE Trans Syst Man Cybern Syst* 51(1):561–573
- Deng Y, Liu X, Fan Y, Zeng Z, Udpa L, Shih W (2006) Characterization of magneto-optic imaging data for aircraft inspection. *IEEE Trans Magn* 42(10):3228–3230
- Gao Y, Tian GY, Li K, Ji J, Wang P, Wang H (2015) Multiple cracks detection and visualization using magnetic flux leakage and eddy current pulsed thermography. *Sens Actuators A Phys* 234:269–281
- He D, Xu K, Zhou P, Zhou D (2019) Surface defect classification of steels with a new semi-supervised learning method. *Opt Lasers Eng* 117:40–48
- Hu G, Huang J, Wang Q, Li J, Xu Z, Huang X (2020) Unsupervised fabric defect detection based on a deep convolutional generative adversarial network. *Text Res J* 90(3–4):247–270
- Hu J, Zhang H, Liu H, Yu X (2021) A survey on sliding mode control for networked control systems. *Int J Syst Sci* 52(6):1129–1147
- Larochelle H, Bengio Y, Louradour J, Lamblin P (2009) Exploring strategies for training deep neural networks. *J Mach Learn Res* 10:1–40
- Li H-J, Bu Z, Wang Z, Cao J, Shi Y (2018) Enhance the performance of network computation by a tunable weighting strategy. *IEEE Trans Emerg Top Comput Intell* 2(3):214–223
- Li Q, Shen B, Wang Z, Sheng W (2020) Recursive distributed filtering over sensor networks on Gilbert-Elliott channels: a dynamic event-triggered approach. *Automatica* 113 (art. no. 108681)
- Li Q, Shen B, Wang Z, Huang T, Luo J (2019) Synchronization control for a class of discrete time-delay complex dynamical networks: a dynamic event-triggered approach. *IEEE Trans Cybern* 49(5):1979–1986
- Li X, Han F, Hou N, Dong H, Liu H (2020) Set-membership filtering for piecewise linear systems with censored measurements under Round-Robin protocol. *Int J Syst Sci* 51(9):1578–1588

20. Liu D, Wang Z, Liu Y, Alsaadi FE (2020) Extended Kalman filtering subject to random transmission delays: dealing with packet disorders. *Inf Fusion* 60:80–86
21. Liu L, Ma L, Zhang J, Bo Y (2021) Distributed non-fragile set-membership filtering for nonlinear systems under fading channels and bias injection attacks. *Int J Syst Sci* 52(6):1192–1205
22. Liu S, Wang Z, Chen Y, Wei G (2020) Dynamic event-based state estimation for delayed artificial neural networks with multiplicative noises: a gain-scheduled approach. *Neural Netw* 132:211–219
23. Liu W, Wang Z, Liu X, Zeng N, Liu Y, Alsaadi FE (2017) A survey of deep neural network architectures and their applications. *Neurocomputing* 234:11–26
24. Liu W, Wang Z, Liu X, Zeng N, Bell D (2018) A novel particle swarm optimization approach for patient clustering from emergency departments. *IEEE Trans Evol Comput* 23(4):632–644
25. Liu W, Wang Z, Yuan Y, Zeng N, Hone K, Liu X (2019) A novel sigmoid-function-based adaptive weighted particle swarm optimizer. *IEEE Trans Cybern* 51(2):1085–1093
26. Liu Y, Cheng Q, Gan Y, Wang Y, Li Z, Zhao J (2019) Multi-objective optimization of energy consumption in crude oil pipeline transportation system operation based on exergy loss analysis. *Neurocomputing* 332:100–110
27. Liu Y, Chen S, Guan B, Xu P (2019) Layout optimization of large-scale oil-gas gathering system based on combined optimization strategy. *Neurocomputing* 332:159–183
28. Liu Y, Wang Z, Ma L, Alsaadi FE (2019) A partial-nodes-based information fusion approach to state estimation for discrete-time delayed stochastic complex networks. *Inf Fusion* 49:240–248
29. Luo X, Liu Z, Jin L, Zhou Y, Zhou M (2021) Symmetric non-negative matrix factorization-based community detection models and their convergence analysis. *IEEE Trans Neural Netw Learn Syst* (in press). <https://doi.org/10.1109/TNNLS.2020.3041360>
30. Luo X, Yuan Y, Zhou M, Liu Z, Shang M (2019) Non-negative latent factor model based on  $\beta$ -divergence for recommender systems. *IEEE Trans Syst Man Cybern Syst* 51(8): 4612–4623
31. Luo X, Zhou M, Li S, Hu L, Shang M (2019) Non-negativity constrained missing data estimation for high-dimensional and sparse matrices from industrial applications. *IEEE Trans Cybern* 50(5):1844–1855
32. Ma Y, Zhong G, Liu W, Wang Y, Jiang P, Zhang R (2021) ML-CGAN: conditional generative adversarial network with a meta-learner structure for high-quality image generation with few training data. *Cogn Comput*. <https://doi.org/10.1007/s12559-020-09796-4>
33. Peng C, Tian Y-C, Yue D (2010) Output feedback control of discrete-time systems in networked environments. *IEEE Trans Syst Man Cybern Part A Syst Hum* 41(1):185–190
34. Qian W, Li Y, Chen Y, Liu W (2020)  $L_2$ - $L_\infty$  filtering for stochastic delayed systems with randomly occurring nonlinearities and sensor saturation. *Int J Syst Sci* 51(13):2360–2377
35. Qian W, Li Y, Zhao Y, Chen Y (2020) New optimal method for  $L_2$ - $L_\infty$  state estimation of delayed neural networks. *Neurocomputing* 415:258–265
36. Tian L, Cheng Y, Yin C, Xia Y, Huang Y, Bai L (2016) Detection of the crack by reducing the influence of the magnetic domain based on the MOI. In: *Proceedings of the IEEE international instrumentation and measurement technology conference, Taipei, Taiwan, May 2016*, pp 1–6
37. Tian L, Cheng Y, Yin C, Ding D, Song Y, Bai L (2017) Design of the MOI method based on the artificial neural network for crack detection. *Neurocomputing* 226:80–89
38. Wang K, Zhang X, Hao Q, Wang Y, Shen Y (2019) Application of improved least-square generative adversarial networks for rail crack detection by AE technique. *Neurocomputing* 332:236–248
39. Wang Z, Healy G, Smeaton AF, Ward TE (2020) Use of neural signals to evaluate the quality of generative adversarial network performance in facial image generation. *Cogn Comput* 12(1):13–24
40. Xu S, Jiang X, Huang J, Yang S, Wang X (2016) Bayesian wavelet PCA methodology for turbomachinery damage diagnosis under uncertainty. *Mech Syst Signal Process* 80:1–18
41. Yi X, Babyn P (2018) Sharpness-aware low-dose CT denoising using conditional generative adversarial network. *J Digit Imaging* 31(5):655–669
42. Yue D, Zhang Y, Tian E, Peng C (2008) Delay-distribution-dependent exponential stability criteria for discrete-time recurrent neural networks with stochastic delay. *IEEE Trans Neural Netw* 19(7):1299–1306
43. Yue W, Wang Z, Chen H, Payne A, Liu X (2018) Machine learning with applications in breast cancer diagnosis and prognosis. *Designs* 2(2):13
44. Zelenyak AM, Schorer N, Sause MG (2018) Modeling of ultrasonic wave propagation in composite laminates with realistic discontinuity representation. *Ultrasonics* 83:103–113
45. Zeng N, Wang Z, Zhang H, Liu W, Alsaadi FE (2016) Deep belief networks for quantitative analysis of gold immunochromatographic strip. *Cogn Comput* 8(4):684–692
46. Zhao Z, Wang Z, Zou L, Guo J (2020) Set-membership filtering for time-varying complex networks with uniform quantisations over randomly delayed redundant channels. *Int J Syst Sci* 51(16):3364–3377
47. Zhang H, Yue D, Dou C, Zhao W, Xie X (2018) Data-driven distributed optimal consensus control for unknown multiagent systems with input-delay. *IEEE Trans Cybern* 49(6):2095–2105
48. Zhang L, Yang F, Zhang YD, Zhu YJ (2016) Road crack detection using deep convolutional neural network. In: *Proceedings of IEEE international conference on image processing, Phoenix, Arizona, Sept 2016*, pp 3708–3712
49. Zhang N, Ye C, Peng L, Tao Y (2019) Novel array eddy current sensor with three-phase excitation. *IEEE Sens J* 19(18):7896–7905
50. Zhang W, Su H, Zhu F, Yue D (2011) A note on observers for discrete-time Lipschitz nonlinear systems. *IEEE Trans Circuits Syst II Express Briefs* 59(2):123–127
51. Zhu P, Yin C, Cheng Y, Huang X, Cao J, Vong CM, Wong PK (2018) An improved feature extraction algorithm for automatic defect identification based on eddy current pulsed thermography. *Mech Syst Signal Process* 113:5–21
52. Zhu K, Hu J, Liu Y, Alotaibi ND, Alsaadi FE, On  $l_2$ - $l_\infty$  output-feedback control scheduled by stochastic communication protocol for two-dimensional switched systems. *Int J Syst Sci* (in press). <https://doi.org/10.1080/00207721.2021.1914768>
53. Zou L, Wang Z, Geng H, Liu X (2021) Set-membership filtering subject to impulsive measurement outliers: a recursive algorithm. *IEEE/CAA J Autom Sin* 8(2):377–388
54. Zou L, Wang Z, Hu J, Liu Y, Liu X, Communication-protocol-based analysis and synthesis of networked systems: Progress, prospects and challenges. *Int J Syst Sci* (in press). <https://doi.org/10.1080/00207721.2021.1917721>
55. Zou L, Wang Z, Han Q-L, Zhou DH (2021) Moving horizon estimation of networked nonlinear systems with random access protocol. *IEEE Trans Syst Man Cybern Syst* 51(5):2937–2948
56. Zou L, Wang Z, Hu J, Zhou DH (2020) Moving horizon estimation with unknown inputs under dynamic quantization effects. *IEEE Trans Autom Control* 65(12):5368–5375